Ascent Optimization for a Heavy Space Launcher

C. Ponssard K. Graichen N. Petit J. Laurent–Varin

***Abstract*— This paper exposes work to optimize the ascent trajectory of a multistage space launcher. Motivated by well–known singular arc effects as in the case of the Goddard rocket, we investigate whether the payload of the launcher can be enhanced by means of a variable thrust during the first phase of the flight. Due to the high complexity and numerical sensitivity of the multistage problem, we use constructive methods for initialization and handling input constraints in optimal control to compute the ascent trajectories. Based on realistic numerical values for key design parameters and flight dynamics, we conclude that the computed trajectories are in fact full thrust.**

INTRODUCTION

In the recent years, variable thrust engine have been considered for space launchers and vehicles, see e.g. [8]. Developing such engines is a major technological achievement which is expected to enable new trajectories for the launchers, which in turn might be able to carry heavier payloads.

Computing the payload capacity of a launcher is usually performed through a trajectory optimization process which incorporates the destination orbit as a terminal state constraint, while accounting for systems dynamics and thrust limitations. Such trajectories have been studied for decades and are often updated to take into account modifications of the launcher and key parameters of the space mission (such as visibility from ground stations), see e.g. [4].

Commonly (see [2]), the thrust of the main boosters at the beginning of the flight is kept constant ("full thrust"), mainly due to technological reasons in view of the huge mass flow and thrust level. Yet, the question arises if a variable thrust engine could lead to an increased payload. This scenario is motivated by singular (sub)arc effects in ascent trajectories, e.g. of launch vehicles [4] or the well–known Goddard problem [5], [10], [11]. These effects indeed indicate that a full–thrust flight might not be optimal.

We consider a flight mission to the geostationary transfer orbit (GTO) for a Ariane 5 launcher as part of the joint OPALE project with *Centre Nationale d'Etudes Spatiales* (CNES). This ascent is composed of three parts which are defined by the use of the main boosters and the first and second stage engines. Without assuming any a-priori thrust law, we design a trajectory which maximizes the payload.

To compute the optimal ascent trajectories, we use an indirect approach in optimal control. Significant problems in this context are the high complexity of the model as well as the high sensitivity of the ascent problem due to the long flight time and the switching between the single flight phases.

To overcome these problems, we employ two recently presented constructive methods that have been applied to the space shuttle reentry problem [6]. In the first step, we consider the full thrust flight and compute the optimal ascent trajectories with a homotopy method, which starts from a suboptimal trajectory that is obtained by forward integration and simple linear input profiles. In the variable thrust scenario, the homotopy method is combined with a saturation function approach to incorporate the thrust level constraints into a new unconstrained formulation. A collocation method under MATLAB is used to solve the multi–point boundary value problems of the optimality conditions.

Realistic value of the key parameters (including tabulated data) in the nonlinear model of the rocket are considered, along with initial conditions corresponding to the launch pad at Kourou in Guyanne. Based on this study, we conclude that the optimal ascent trajectory actually corresponds to a full thrust control law for the main boosters. Although it seems that a variable thrust engine does not lead to better ascent trajectories or a higher payload for the given parameters, it is expected that further changes in the launcher design will yield more interest in the possibility of varying the thrust of the main engine.

I. PROBLEM STATEMENT

The problem under consideration in this paper is the trajectory optimization for a heavy launcher (e.g. Ariane 5) from the surface of the Earth to a geostationary transfer orbit (GTO). This final orbit is used to put satellites into geostationary orbit (GEO). Therefore, the cost to be maximized here is the payload of the launcher.

A. Description of phases

The ascent of the launcher consists of the following three phases which determine the order of separation and ignition of the main boosters and the Stage 1 and 2 engines.

- **Phase 1** uses the main boosters and the first stage. The main boosters are separated after the fuel is consumed.
- **Phase 2** still uses the first stage until the respective fuel is consumed and the first stage is separated.
- **Phase 3** is outside the atmosphere. The second stage is ignited and places the payload into the orbit.

The switching times between the single phases and the overall flight time are implicitly determined by the masses in the boosters and are described in more detail in Section I-E.

B. Flight dynamics

The flight dynamics of the launcher are modeled with

$$\dot{r} = v, \quad \dot{v} = \frac{1}{\bar{m}} \left[T(r,u) - D(r,v) \right] + g(r) \,, \qquad (1)$$

where $r \in \mathbb{R}^3$ and $v \in \mathbb{R}^3$ are the position and velocity with respect to the geocentric frame. The input vector u consists of the (assumed) variable thrust level $\alpha \in [0,1]$ of the launcher and the orientation of the rocket:

$$u = \begin{cases} \alpha \in [0,1] & \text{normalized thrust level,} \\ \theta \in [-\pi,\pi] & \text{heading} \\ \psi \in [-\pi,\pi] & \text{azimuth} \end{cases} \qquad (2)$$

This work was partially supported by Centre Nationale d'Etudes Spatiales (CNES) through the OPALE R&T project.

C. Ponssard is with ENSTA clement.ponssard@ensta.fr
K. Graichen is with TU Wien graichen@acin.tuwien.ac.at
N. Petit is with MINES ParisTech nicolas.petit@ensmp.fr
J. Laurent–Varin is with CNES julien.laurent-varin@cnes.fr

ISBN 978-963-311-369-1

The details behind the overall mass $\bar{m}$, the thrust $T(r,u)$, the drag $D(r,v)$, and the gravity $g(r)$ are given in the following. For the symbols and constants which will be used we refer to Table I together with their respective numerical values.

1) Thrust: The thrust in (1) is defined by

$$T(r,u) := |T(r,\alpha)| \cdot \mathrm{dir}\big(T(r,\theta,\psi)\big)\,. \tag{3}$$

The norm of the thrust depends on which boosters are active in the single phases [1]

$$|T(r,\alpha)| = \begin{cases} (\alpha\beta_1 I_{\mathrm{SP},1}+\beta_2 I_{\mathrm{SP},2})g_0 & \\ \qquad -(S_1+S_2)P_{\mathrm{z}}(h) & \text{Phase 1} \\ \beta_2 I_{\mathrm{SP},2} g_0 - S_2 P_{\mathrm{z}}(h) & \text{Phase 2} \\ \beta_3 I_{\mathrm{SP},3} g_0 & \text{Phase 3} \end{cases} \tag{4}$$

The direction of the thrust is defined by the two controlled angles θ and ψ

$$\mathrm{dir}(T\big(r,\theta,\psi)\big) = \begin{pmatrix} -\sin\theta\sin\psi\sin\phi + \cos\theta\cos\phi \\ \sin\theta\cos\psi \\ \sin\theta\sin\psi\cos\phi + \cos\theta\sin\phi \end{pmatrix}$$

with $\cos\phi = \sqrt{r_1^2+r_2^2}/|r|$ and $\sin\phi = r_3/|r|$.

2) Drag forces: We consider a vector equation to define the drag forces, based on a calculation of the relative wind speed

$$D(r,v) = -qS_r C_x(M)\frac{V_{\mathrm{rel}}}{|V_{\mathrm{rel}}|}\,, \tag{5}$$

$$\begin{aligned} q &= \frac{1}{2}\gamma P_{\mathrm{z}}(h) M^2 && \text{dynamic pressure} \\ V_{\mathrm{rel}} &= v - V_{\mathrm{air}} = v - \begin{pmatrix} -r_2 \\ r_1 \\ 0 \end{pmatrix}\Omega_{\mathrm{Earth}} && \text{relative speed} \\ M &= |V_{\mathrm{rel}}|/V_{\mathrm{s}}(h) && \text{Mach number} \end{aligned}$$

The speed of sound $V_{\mathrm{s}}(h)$ and the atmospheric pressure $P_{\mathrm{z}}(h)$ depend on the altitude $h = |r| - R_{\mathrm{Earth}}$.

TABLE I
SYMBOLS AND DATA OF THE LAUNCHER PROBLEM.

Symbol	Description	Unit	value
R_{Earth}	Radius of the Earth	m	6378135
μ	Gravitational constant	$\mathrm{m}^3/\mathrm{s}^2$	$3.98602 \cdot 10^{14}$
J_2	Dynamic shape factor	-	0.0010826
Ω_{Earth}	Rotation period	s^{-1}	$7.274854 \cdot 10^{-5}$
g_0	Gravity constant	$\mathrm{m/s}^2$	9.81
γ	Heat capacity ratio	-	1.4
$I_{\mathrm{SP},i}$, $i=1,2,3$	Specific impulse	s	
$m_{\mathrm{net},i}$, $i=1,2,3$	Stages net masses	kg	$(2{\cdot}38, 17, 6.2){\cdot}10^3$
β_i, $i=1,2,3$	Mass outflows	kg/s	$(2\cdot 2000, 320, 40)$
S_i, $i=1,2,3$,	Fuel outlet area	m^2	$(2\cdot 7, 3.6, 0)$
m_{hood}	Launcher hood mass	kg	$2\cdot 10^3$
S_r	Aerodyn. ref. surface	m^2	23.345
m	Total mass	kg	
$T(r,u)$	Total thrust	N	
$D(r,v)$	Drag forces	N	
$g(r)$	Gravity	$\mathrm{m/s}^2$	
q	Dynamic pressure		
S_r	Drag force ref. area	m^2	
C_x	Drag coefficient		
V_{rel}	Relative speed	m/s	
M	Mach number		
V_{s}	Speed of sound	m/s	
P_z	Atmospheric pressure	Pa	

[1] The values of the specific impulses in Table I are omitted for confidentiality reasons.

3) Gravity: The gravity is computed using the J_2 effect due to the non-sphericity of the Earth. This gives

$$g(r) = -\frac{\mu}{|r|^3}(r + J_2\frac{R_{\mathrm{Earth}}^2}{|r|^2}M_{J_2} r) \tag{6}$$

with $M_{J_2} = \begin{pmatrix} 1-5\frac{r_3^2}{|r|^2} & 0 & 0 \\ 0 & 1-5\frac{r_3^2}{|r|^2} & 0 \\ 0 & 0 & 3-5\frac{r_3^2}{|r|^2} \end{pmatrix}$

4) Numerical data: Both the speed of sound $V_s(h)$ (m/s) and the atmospheric pressure $P_z(h)$ (Pa) have been tabulated as function of the altitude h (m) under the form of twice differentiable lookup tables. In addition, the dimensionless drag coefficient $C_x(M)$ is a tabulated function of the Mach number M.

C. Mass balances

The overall mass $\bar{m}$ of the launcher in (1) consists of the payload m_{load} and the masses of the boosters depending on the respective flight phase:

$$\bar{m} = m_{\mathrm{load}} + \begin{cases} m_{\mathrm{hood}} + \sum_{i=1}^{3}(m_{\mathrm{net},i} + m_i) & \text{Phase 1} \\ m_{\mathrm{hood}} + \sum_{i=2}^{3}(m_{\mathrm{net},i} + m_i) & \text{Phase 2} \\ m_{\mathrm{net},3} + m_3 & \text{Phase 3} \end{cases} \tag{7}$$

The hood for the heat protection during the ascent is separated after the second phase, when the rocket is outside the atmosphere. The symbols $m_{\mathrm{net},i}$ denote the net masses of the main boosters, the first and second stage, respectively.

The dynamics of the masses $m = (m_1, m_2, m_3)^{\mathsf{T}}$

$$\dot{m} = f_m(\alpha) \tag{8a}$$

are modeled phase–dependently by

	Phase 1	Phase 2	Phase 3
$f_{m,1} =$	$-\alpha\beta_1$	0	0
$f_{m,2} =$	$-\beta_2$	$-\beta_2$	0
$f_{m,3} =$	0	0	$-\beta_3$

(8b)

where β_i is the fuel mass outlet of the main boosters, the first stage engine and the second stage engine, respectively.

The separate consideration of the masses has the advantage that the state variables m_i are continuous over the switching times between the phases, although the overall mass (7) will be discontinuous. [2]

D. Boundary conditions

The launch point is Kourou. The initial speed of the launcher is given by the rotation of the Earth. In addition, the initial fuel masses are given according to standard values.

The actual optimization phase starts 22.3 s after the actual take–off. This time interval correspond to a specified flight strategy which incorporates the initialization of the inertial measurement units (7.3 s) and initial vertical flight times with 5 s and 10 s at full thrust to leave the launch zone as soon as possible. Taking all these factors into account and

[2] As a consequence, the corresponding adjoint states of the optimality conditions (see Section II-B) are also continuous over the switching times [9].

performing a simple time shift to cancel the 22.3 s offset, we consider the initial conditions to our trajectory optimization problem

$$\begin{aligned} r(0) &= (6352342, 12216, 578716)\,\mathrm{m} \\ v(0) &= (89.9981, 472.8553, 8.1846)\,\mathrm{m/s} \\ m(0) &= (408.2\cdot 10^3, 165.88\cdot 10^3, 28\cdot 10^3)\,\mathrm{kg} \end{aligned} \tag{9}$$

The final conditions at the end of the flight time t_f follow from some of the orbital elements defining the GTO. Using Keplerian coordinates

$$\begin{aligned} a_{\mathrm{GTO}} &= 2.4290635\cdot 10^7 && \text{semi major axis} \\ e_{\mathrm{GTO}} &= 0.728161 && \text{excentricity} \\ i_{\mathrm{GTO}} &= 0.122172 && \text{inclination} \end{aligned} \tag{10}$$

the final conditions for r and v are given by a nonlinear vector function

$$\Psi(r(t_f), v(t_f)) = (a, e, i)^{\mathsf{T}}_{\mathrm{GTO}} \tag{11}$$

where $\Psi : \mathbb{R}^6 \to \mathbb{R}^3$ maps r, v to the Keplerian coordinates (a, e, i). The standard orbit relations in Ψ are omitted here due to the lack of space.

E. Switching between the flight phases

The switching times between the single phases, t_1 and t_2, are implicitly defined. Phase 1 lasts until the mass contained in the main boosters has reached a critical value $m_{\mathrm{crit},1}$. Then Phase 2 lasts until m_2 has reached a corresponding safety value $m_2(t_2) = m_{\mathrm{crit},2}$. Eventually, Phase 3 lasts until the GTO is reached and $m_3(t_3) = m_{\mathrm{crit},3}$. These conditions implicitly define the switching times t_1, t_2, and the final time t_f according to

$$\begin{aligned} m_1(t_1) &= m_{\mathrm{crit},1} \\ m_2(t_2) &= m_{\mathrm{crit},2} \\ m_3(t_f) &= m_{\mathrm{crit},3}. \end{aligned} \tag{12}$$

In the simulations, the critical mass of the main boosters is set to $m_{\mathrm{crit},1} = 23.4\,\mathrm{tons}$, whereas no critical masses are considered for the Stage 1 and 2 engines, i.e. $m_{\mathrm{crit},2} = m_{\mathrm{crit},3} = 0$.

II. Full thrust trajectory optimization

In the first step we consider the full thrust flight ($\alpha = 1$) in order to present a homotopy approach, which is used throughout all the numerical experiments reported in this paper. The section starts with summarizing the optimal control problem with full thrust before the homotopy approach is presented to overcome the well–known problem of finding a suitable initial guess for the adjoint variables occuring in the optimality conditions of the launcher problem.

A. Optimal control problem

As stated before, the goal of the ascent problem is to maximize the payload m_{load}. Summarizing the results from the previous section and keeping in mind that at this stage we fix the thrust level $\alpha = 1$, the optimal control problem for the launcher (called $\mathrm{OCP}_{\alpha=1}$) takes the form

$$\mathrm{OCP}_{\alpha=1}\begin{cases} \text{Minimize:} & J(u) := -m_{\mathrm{load}} \\ \text{Controls:} & u = (\theta, \psi)^{\mathsf{T}} \\ \text{States:} & x = (r^{\mathsf{T}}, v^{\mathsf{T}}, m^{\mathsf{T}})^{\mathsf{T}} \\ \text{Dynamics (1), (8):} & \dot{x} = f(x, u) \\ \text{Initial cond. (9):} & x(0) = x_0 \\ \text{Continuity cond.:} & x(t_i^-) = x(t_i^+),\ i = 1, 2 \\ \text{Final cond. (11):} & \Psi(x(t_f)) = (a, e, i)^{\mathsf{T}}_{\mathrm{GTO}} \end{cases}$$

The continuity conditions of $\mathrm{OCP}_{\alpha=1}$ at the switching times t_1 and t_2 are necessary to ensure continuity of the states. Also note that in the full thrust case ($\alpha = 1$), t_1, t_2, and t_f can be explicitly determined from (8) and (12). The constraints on the controls (θ, ψ) are rather conservative, see (2), and are not explicitly considered, since the control trajectories stay within reasonable limits. [3].

B. Optimality conditions

In order to express $\mathrm{OCP}_{\alpha=1}$ in the calculus of variations we introduce the payload to be minimized as additional state variable with the trivial ODE

$$\dot{m}_{\mathrm{load}} = 0 \tag{13}$$

and extend the state vector $\bar{x} = (r^{\mathsf{T}}, v^{\mathsf{T}}, m^{\mathsf{T}}, m_{\mathrm{load}})^{\mathsf{T}} \in \mathbb{R}^{10}$. Next, consider the Hamiltonian

$$\begin{aligned} H(x, \lambda, u) = \langle \lambda_r, v\rangle + \left\langle \lambda_v, \frac{1}{m}[T(r, u) - D(r, v)] + g(r) \right\rangle \\ + \langle \lambda_m, f_m(\alpha = 1)\rangle \end{aligned}$$

with the adjoint variables $\lambda = (\lambda_r^{\mathsf{T}}, \lambda_v^{\mathsf{T}}, \lambda_m^{\mathsf{T}}, \lambda_{\mathrm{load}})^{\mathsf{T}} \in \mathbb{R}^{10}$.

The calculus of variations yields the stationarity condition

$$\frac{\partial H}{\partial u} = \frac{1}{m}\langle \lambda_v, T_u\rangle = 0 \tag{14}$$

and the differential equations $\dot{\lambda}^T = -\frac{\partial H}{\partial x}$ which are

$$\dot{\lambda}_r = \big[\frac{1}{m}(D_r^{\mathsf{T}} - T_r^{\mathsf{T}}) - g_r^{\mathsf{T}}\big]\lambda_v \tag{15a}$$

$$\dot{\lambda}_v = \lambda_r + \frac{1}{m}D_v^{\mathsf{T}}\lambda_v \tag{15b}$$

$$\dot{\lambda}_{m,i} = \frac{1}{m^2}\frac{\partial m}{\partial m_i}\langle \lambda_v, T - D\rangle\,, \quad i = 1, 2, 3 \tag{15c}$$

$$\dot{\lambda}_{\mathrm{load}} = \frac{1}{m^2}\langle \lambda_v, T - D\rangle\,. \tag{15d}$$

The partial derivative $\frac{\partial m}{\partial m_i}$ follows from (7) and evaluates to 0 or 1 depending on the current phase of the flight.

The orbit conditions (11) defines an implicit final condition for r and v. Following the standard calculus of variations, this leads to $\lambda_r^{\mathsf{T}}(t_f) = \frac{\partial \Psi}{\partial r}\mu$ and $\lambda_v^{\mathsf{T}}(t_f) = \frac{\partial \Psi}{\partial v}\mu$. The additional Lagrange multiplier μ can be avoided by combining both conditions in one single implicit final condition

$$\lambda_r^{\mathsf{T}} = \frac{\partial \Psi}{\partial r}\left(\frac{\partial \Psi}{\partial v}\right)^{-1}\lambda_v^{\mathsf{T}}\,. \tag{16a}$$

Since no final conditions are imposed on the masses m_i, $i = 1, 2, 3$, we have the corresponding trivial final conditions in the adjoint states

$$\lambda_{m,i}(t_f) = 0\,, \quad i = 1, 2, 3\,. \tag{16b}$$

[3]For the Ariane ascent optimization, the dynamic pressure is not constrained. Yet, its value is typically monitored during the flight for safety reasons.

The benefit of introducing m_{load} as additional state variable becomes clear at this point: the unspecified initial condition $m_{\text{load}}(0)$ and the optimization goal of minimizing $m_{\text{load}}(t_f)$ leads to

$$\lambda_{\text{load}}(0) = 0\,, \quad \lambda_{\text{load}}(t_f) = -1\,. \tag{16c}$$

In summary, we have 20 initial and final conditions in (9), (11), and (16) for the 20 states $\bar{x}$ and λ.

What remains are the interior continuity conditions at the switching times t_1 and t_2 between the flight phases 1 and 2. Table II summarizes the overall set of initial, interior, and final conditions.

TABLE II
BOUNDARY CONDITIONS FOR THE ASCENT PROBLEM.

$t = 0:$	$x(0) = x_0,$	see (9)
	$\lambda_{\text{load}}(0) = 0$	
$t = t_1:$	$\bar{x}(t_1^-) = \bar{x}(t_1^+),$	$i \in \{1..6, 8..10\}$
	$m_1(t_1^+) = m_{\text{crit},1}$	
	$\lambda(t_1^-) = \lambda(t_1^+)$	
$t = t_2:$	$\bar{x}(t_2^-) = \bar{x}(t_2^+),$	$i \in \{1..7, 9..10\}$
	$m_2(t_2^-) = m_{\text{crit},2}$	
	$\lambda(t_2^-) = \lambda(t_2^+)$	
$t = t_f:$	$\Psi(x(t_f)) = (a, e, i)^{\mathsf{T}}_{\text{GTO}}$	
	$m_3(t_f) = m_{\text{crit},3}$	
	$\lambda_r^{\mathsf{T}} = \frac{\partial \Psi}{\partial r}\left(\frac{\partial \Psi}{\partial v}\right)^{-1}\lambda_v^{\mathsf{T}}$	
	$\lambda_{\text{load}}(t_f) = -1$	

C. Homotopy approach for adjoint initialization

The computation of the optimal ascent trajectories requires the solution of the boundary value problem defined by (1), (8), (14), (15) with the boundary conditions in Table II. A well–known problem in this context is the sensitivity of the solution with respect to the initial guess of the adjoint states λ. This problem is particularly present in our case, since the overall time t_f for the ascent problem is considerably long. The switching conditions further complicate the situation.

There exist various numerical approaches which address the initial guess problem of the adjoint states, e.g. based on collocation [3] or the combination of direct/indirect methods [12]. We will alternatively use a homotopy approach which was already successfully applied to the reentry problem of the space shuttle [6]. To simplify matters, the approach is presented using the compact notation of $\text{OCP}_{\alpha=1}$ without going into detail with the structure of the dynamics and final conditions.

In the first step, assume that an initial trajectory $(x^0(t), u^0(t)),\ t \in [0, t_f]$ over the whole flight time t_f is known, which satisfies the system equations and initial conditions

$$\dot{x}^0 = f(x^0, u^0), \quad x^0(0) = x_0\,. \tag{17}$$

In general, the rocket will not reach the desired GTO for this "guessed" input trajectory. The orbit conditions (11) will instead evaluate to certain orbit values

$$\Psi(x(t_f^0)) = \Psi^0\,. \tag{18}$$

In our case, this initial trajectory will be obtained by a forward integration in time (see Section II-D).

The trajectory $(x^0(t), u^0(t)),\ t \in [0, t_f]$ can now be used to modify the cost functional and orbit conditions of $\text{OCP}_{\alpha=1}$ according to

$$J(u) := -c\, m_{\text{load}} + (1-c)\int_0^{t_f} |u(t) - u^0(t)|^2 \mathrm{d}t \tag{19}$$

$$\Psi(x(t_f)) = c\,(a, e, i)^{\mathsf{T}}_{\text{GTO}} + (1-c)\Psi^0 \tag{20}$$

with the homotopy parameter $c \in [0, 1]$. Obviously, $c = 1$ corresponds to $\text{OCP}_{\alpha=1}$, whereas $c = 0$ suppresses the payload term in (19) and the GTO parameters in the final conditions (20), such that the initial trajectory $(x^0(t), u^0(t)),\ t \in [0, t_f]$ is exactly the optimal solution for $c = 0$.

For $c = 0$ the trivial adjoint states $\lambda^0(t) = 0$ together with $x^0(t), u^0(t),\ t \in [0, t_f]$ solve the optimality conditions (14) and (15) extended by the addition terms in (19) and (20), see [6]. Hence, $(\lambda^0 = 0, x^0, u^0)$ can be used as an initial guess of the OCP solution with $c^0 = 0$ and using a continuation scheme with an increasing sequence $0 = c^0 < c^1 < \cdots < c^N = 1$ to eventually recover the original $\text{OCP}_{\alpha=1}$. For details on the homotopy approach we refer to [6] and directly apply the method to the solution of the ascent problem.

D. Numerical solution

The multi–point boundary value problem consisting of the dynamics (1), (8), (15), the algebraic equations (14) and the boundary conditions in Table II is solved with a collocation code under MATLAB.[4] The optimality conditions (14) and (15) are derived using MATHEMATICA and are exported to MATLAB as optimized Cmex functions.

Figure 1 shows the optimal trajectories of the homotopy solution for an initial input trajectory $u^0(t) = (\theta^0, \psi^0)(t),\ t \in [0, t_f]$ with a linear interpolation between 30 deg and 140 deg for $\theta^0(t)$ and zero for $\psi^0(t)$. The initial value of the payload is set to $m_{\text{load}} = 10$ tons. This payload and the initial trajectory roughly correspond to realistic scenarios.[5] Nevertheless, the initial state trajectory $x^0(t)$ clearly deviates from the optimal solution for $c = 1$ (cf. the altitude trajectory in Fig. 1), which shows both the sensitivity of the problem and the robustness of the homotopy approach.

The homotopy solution from $c = 0$ to $c = 1$ was obtained in five equally spaced steps from $c^1 = 0.2$ to $c^5 = 1$. Figure 1 also shows the trajectories for $c = 0.99$ to illustrate the strong change in the trajectories at the end of the homotopy.[6]

Figure 2 shows the overall mass of the rocket during the ascent. Clearly visible are the switching times t_1 and t_2, where the main boosters and the stage 1 engines are separated. In addition, Fig. 3 shows the flight trajectory with respect to the Earth surface.

We obtain a payload $m_{\text{load}} = 12.11$ tons for $c = 1$. Interestingly, the obtained trajectory is somewhat different from known references trajectories while providing similar

[4] To cope with (index 1) DAEs as they typically arise in optimal control, the standard MATLAB BVP solver bvp4c was modified by the authors to account for additional algebraic equations.

[5] The trajectories of the altitude and velocity are shown dimension–free for confidentiality reasons.

[6] The solution time under MATLAB for each homotopy step was between 4-9 seconds with a fixed time mesh of 180 points.

values. The mentioned trajectories usually incorporate other constraints such as, e.g., visibility from ground radar stations.

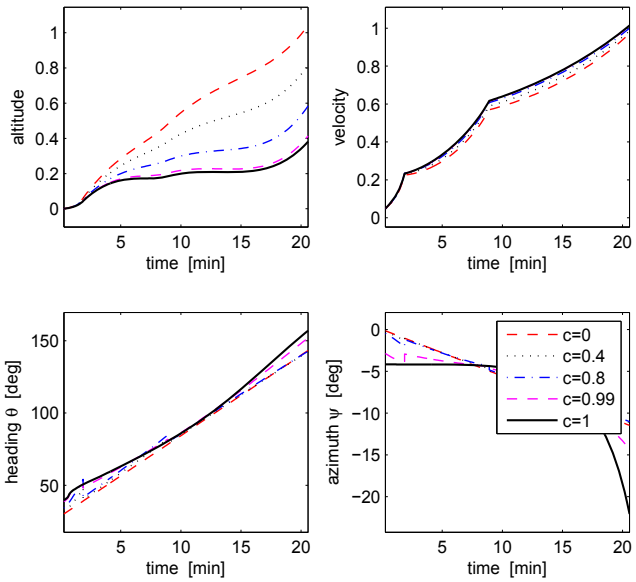

Fig. 1. Optimal homotopy trajectories with full thrust ($\alpha = 1$).

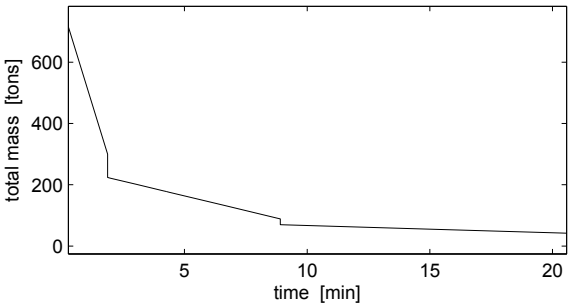

Fig. 2. Overall mass (7) of the launcher during the ascent with full thrust.

III. Variable Thrust Trajectory Optimization

We now turn to the main problem of interest of this paper. Using the same methodology as the one presented for the fixed thrust trajectory optimization, we consider the parameter α which can freely vary within the interval $[0,\ 1]$.

This scenario is motivated by ascent problems such as the well–known Goddard problem [5], [10], where a singular arc appears in the optimal thrust trajectory for maximizing the altitude. Hence, the question arises if an additional singular arc can be detected in the thrust trajectory of the launcher problem, which would lead to a higher payload compared to the full thrust flight.

The optimal control problem (called $\mathrm{OCP}_{\alpha\le 1}$) is

$$\mathrm{OCP}_{\alpha\le 1}\left\{\begin{array}{ll} \text{Minimize:} & J(u) := -m_{\mathrm{load}} \\ \text{Controls:} & u = (\alpha,\theta,\psi)^{\mathsf{T}} \\ \text{States:} & x = (r^{\mathsf{T}}, v^{\mathsf{T}}, m^{\mathsf{T}})^{\mathsf{T}} \\ \text{Dynamics (1), (8):} & \dot{x} = f(x,u) \\ \text{Constraints:} & 0 \le \alpha \le 1 \\ \text{Initial cond. (9):} & x(0) = x_0 \\ \text{Continuity cond.:} & x(t_i^-) = x(t_i^+),\ i = 1,2 \\ \text{Final cond. (11):} & \Psi(x(t_f)) = (a,e,i)^{\mathsf{T}}_{\mathrm{GTO}} \end{array}\right.$$

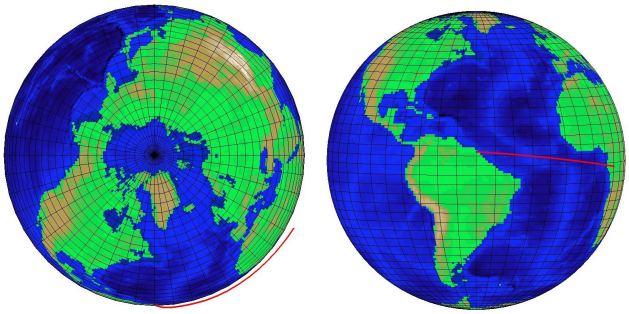

Fig. 3. Flight path of the launcher (red profile).

Note that the first switching time t_1 is now implicitly defined by the condition in (12) and cannot be calculated beforehand as in the full–thrust case. The second switching time t_2 and the final time t_f, however, can be computed with respect to t_1, since the thrust of the Stage 1 and 2 engines remains constant.

A. Saturation function approach

The approach that we use to account for the thrust constraints has been presented in [6] and applied to the reentry problem in the same paper. The idea is to replace the constrained control $\alpha \in [0,1]$ by a smooth saturation function

$$\alpha = \Phi(\tilde{\alpha}) \tag{21}$$

with $\Phi : \mathbb{R} \to (0,1)$ and the new unconstrained control $\tilde{\alpha}$, see Fig. 4. With this input transformation, the previous $\mathrm{OCP}_{\alpha\le 1}$ is replaced by a new unconstrained $\mathrm{OCP}^{\varepsilon}_{\tilde{\alpha}}$

$$\mathrm{OCP}^{\varepsilon}_{\tilde{\alpha}}\left\{\begin{array}{ll} \text{Minimize:} & \tilde{J}(\tilde{u}) := -m_{\mathrm{load}} + \displaystyle\int_0^{t_f} \varepsilon\,\tilde{\alpha}^2\,\mathrm{d}t \\ \text{Controls:} & \tilde{u} = (\tilde{\alpha},\theta,\psi)^{\mathsf{T}} \\ \text{States:} & x = (r^{\mathsf{T}}, v^{\mathsf{T}}, m^{\mathsf{T}})^{\mathsf{T}} \\ \text{Dynamics (1), (8):} & \dot{x} = \tilde{f}(x,\tilde{u}) \\ \text{Initial cond. (9):} & x(0) = x_0 \\ \text{Continuity cond.:} & x(t_i^-) = x(t_i^+),\ i = 1,2 \\ \text{Final cond. (11):} & \Psi(x(t_f)) = (a,e,i)^{\mathsf{T}}_{\mathrm{GTO}} \end{array}\right.$$

where the dynamics function $\tilde{f}(x,\tilde{u})$ follows from (1), (8) by substituting $\alpha = \Phi(\tilde{\alpha})$.

It is shown in [6] that constrained arcs of $\mathrm{OCP}_{\alpha\le 1}$ (i.e. an active constraint $\alpha = 0$ or $\alpha = 1$) corresponds to a singular arc in $\mathrm{OCP}^{\varepsilon}_{\tilde{\alpha}}$. To account for this point and to preserve regularity of $\mathrm{OCP}^{\varepsilon}_{\tilde{\alpha}}$, an additional regularization term $\varepsilon\alpha^2$ is introduced in the running cost of $\mathrm{OCP}^{\varepsilon}_{\tilde{\alpha}}$. The parameter $\varepsilon > 0$ has to be reduced in a sequence $\{\varepsilon_k\}$ of solutions with $\varepsilon_k < \varepsilon_{k-1}$ in order to approach the desired constrained ascent trajectories.

Note that the regularization term $\varepsilon\tilde{\alpha}^2$ is equivalent to a barrier penalty in the original $\mathrm{OCP}_{\alpha\le 1}$ as elaborated in [6]. In this context, the saturation function formulation has the advantage that the constraint $\alpha \in [0,1]$ is strictly satisfied and does not suffer from the numerical sensitivity of barrier penalty methods, where special attention has to be paid to not violating the barriers. This problem is avoided by the saturation function approach at the expense that the new input $\tilde{\alpha}$ will approach infinity in the limit $\varepsilon \to 0$. More information on these properties can be found in [6], [7].

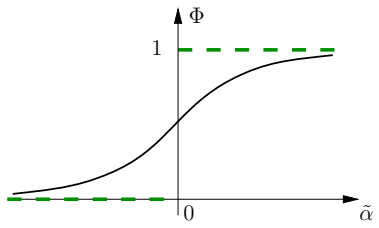

Fig. 4. Smooth saturation function Φ with new unconstrained input $\tilde{\alpha}$.

B. Numerical results

Similar to the full thrust case, the ascent trajectories are calculated via the homotopy approach starting from the same initial input trajectory as in Section II-D and taking $\tilde{\alpha}^0(t) = 0.9$.[7] The regularization parameter is set to $\varepsilon = 10^{-3}$.

In contrast to the full thrust case, the first switching time t_1 is unspecified due to the variable fuel outlet of the main boosters. This is taken into account by adding the interior condition $m_1(t_1^-) = m_{\text{crit},1}$ to the boundary conditions in Table II and performing a time transformation $t = \delta\tau$, where $\tau \in [0, t_1']$ with the fixed switching time t_1' corresponds to the full thrust case. The time scaling δ is considered as free parameter in the collocation solver.

At the end of the homotopy solution, the ascent trajectories for $\text{OCP}_{\tilde{\alpha}}^{\varepsilon}$ with $\varepsilon = 10^{-3}$ are obtained, which is the actual start of the variable thrust considerations. In order to approach the actual optimal solution, the regularization parameter was successively reduced from $\varepsilon = 10^{-3}$ to $\varepsilon = 10^{-10}$ in 9 steps and using the previous trajectories to re–initialize the collocation solver. Figure 5 shows the ascent trajectories with variable thrust for several values of ε.

Obviously, the variable thrust scenario yields the same optimal trajectories as in the full thrust case with a maximal payload of $m_{\text{load}} = 12.11$ tons for $\varepsilon = 10^{-10}$. During the first flight phase in Fig. 5, the internal new input $\tilde{\alpha}(t)$ increases in value for decreasing ε, which in turn implies that the thrust trajectory $\alpha(t)$ following from the saturation function (21) approaches the upper constraint $\alpha = 1$.

We conclude from these results that no singular arc can be found in the ascent problem for the given physical values.

IV. Conclusions

The results of the presented study are in accordance with those determined by a rather different approach in [9]. For the considered physical parameters of the launcher, the (at least local) optimal solution does not present any singular arc. In conclusion, the thrust must be used at this maximum until the fuel is consumed. This property seems to stem from the relatively low aerodynamics forces that are applied to the launcher. It is reported in [9] that short singular arcs (typically a few seconds) could be obtained with substantially different aerodynamics parameters. These small duration arcs are actually difficult to detect. Indeed, a dedicated mesh refinement strategy should probably be developed to make sure that the two point boundary solver can represent and find them by a collocation method. This point is currently under consideration. Another point of interest which is under study is the incorporation of a dynamic pressure constraint (as in the atmospheric reentry problem [1]). This mixed input-state constraint could be accounted for following the same saturation function approach used in [6].

[7] This value corresponds to a thrust level α of approximately 0.98 using exponential functions to construct (21).

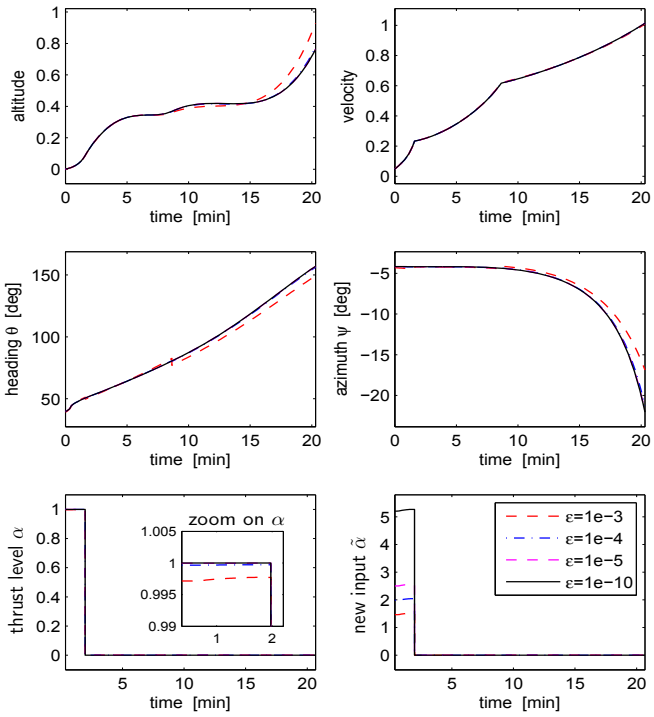

Fig. 5. Optimal trajectories for the variable thrust problem ($\alpha \leq 1$) for decreasing regularization parameters ε.

References

[1] J.T. Betts. *Practical Methods for Optimal Control Using Nonlinear Programming*. Society for Industrial and Applied Mathematics (SIAM), Philadelphia, PA, 2001.

[2] H. Burkhardt, M. Sippel, A. Herbertz, and J. Klevanski. Comparative study of kerosene and methane propellant engines for reusable liquid booster stages. In *4th Int. Conf. Launcher Techn.*, 2002.

[3] A.J. Caliste, M. Melamed, and S. Lee. Design and evaluation of a three-dimensional optimal ascent guidance algorithm. *J. Guid. Contr. Dyn.*, 21(6):867–875, 1998.

[4] P. F. Gath and A. J. Calise. Optimization of launch vehicle ascent trajectories with path constraints and coast arcs. *J. Guid. Contr. Dyn.*, 24(2):296–304, 2001.

[5] R.H. Goddard. A method for reaching extreme altitudes. *Smithsonian Miscellaneous Collections 71*, 1919.

[6] K. Graichen and N. Petit. Constructive methods for initialization and handling mixed state-input constraints in optimal control. *J. Guid. Contr. Dyn.*, 31(5):1334–1343, 2008.

[7] K. Graichen and N. Petit. Incorporating a class of constraints into the dynamics of optimal control problems. *Opt. Contr. Appl. Meth.* (in press), 2009.

[8] B. M. Kiforenko, Z. V. Pasechnik, and I. Y. Vasil'ev. Comparison of the rocket engines efficiency in the case of low thrust orbit-to-orbit transfers. *Acta Astronautica*, 60:801–809, 2007.

[9] P. Martinon, F. Bonnans, J. Laurent-Varin, and E. Trélat. Numerical study of optimal trajectories with singular arcs for space launcher problems. *J. Guid. Contr. Dyn.* (accepted), 2008.

[10] H. Seywald and E.M. Cliff. Goddard problem in presence of a dynamic pressure limit. *J. Guid. Contr. Dyn.*, 16:776–781, 1992.

[11] P. Tsiotras and H. J. Kelley. Drag-law effect in the Goddard problem. *Automatica*, 27(3):481–490, 1991.

[12] O. von Stryk and R. Bulirsch. Direct and indirect methods for trajectory optimization. *Ann. Oper. Res.*, 37:357–373, 1992.